RAPID COMMUNICATIONS IN MASS SPECTROMETRY
Rapid Commun. Mass Spectrom. 2009; **23**: 2741–2753
Published online in Wiley InterScience (www.interscience.wiley.com) DOI: 10.1002/rcm.4183

RCM

Spectral characterisation of eight glycerolipids and their detection in natural samples using time-of-flight secondary ion mass spectrometry

Christine Heim[1]*, Peter Sjövall[2], Jukka Lausmaa[2], Tim Leefmann[1] and Volker Thiel[1]

[1]Geobiology Group, Geoscience Centre, University of Göttingen, Goldschmidtstraße 3, D-37077 Göttingen, Germany
[2]Chemistry and Materials Technology, SP Technical Research Institute of Sweden, P.O. Box 857, SE-50115 Borås, Sweden

Received 20 March 2009; Revised 20 May 2009; Accepted 29 June 2009

In recent years, time-of-flight secondary ion mass spectrometry (ToF-SIMS) with cluster ion sources has opened new perspectives for the analysis of lipid biomarkers in geobiology and organic geochemistry. However, published ToF-SIMS reference spectra of relevant compounds are still sparse, and the influence of the chemical environment (matrix) on the ionisation of molecules and their fragmentation is still not well explored. This study presents ToF-SIMS spectra of eight glycerolipids as common target compounds in biomarker studies, namely ester- and ether-bound phosphatidylethanolamine, ester- and ether-bound phosphatidylcholine, ester-bound phosphatidylglycerol, ester- and ether-bound diglycerides and archaeol, obtained with a Bi_3^+ cluster ion source. For all of these compounds, the spectra obtained in positive and negative analytical modes showed characteristic fragments that could clearly be assigned to e.g. molecular ions, functional groups and alkyl chains. By comparison with the reference spectra, it was possible to track some of these lipids in a pre-characterised organic extract and in cryosections of microbial mats. The results highlight the potential of ToF-SIMS for the laterally resolved analysis of organic biomarkers in environmental materials. The identification of the target compounds, however, may be hampered by matrix effects (e.g. adduct formation) and often require careful consideration of all spectral features and taking advantage of the molecular imaging capability of ToF-SIMS. Copyright © 2009 John Wiley & Sons, Ltd.

Time-of-flight secondary ion mass spectrometry (ToF-SIMS) is a surface analysis technique that allows simultaneous analysis of inorganic and organic molecules on solid surfaces.[1,2] During the last 10–20 years, ToF-SIMS has been used mainly in material sciences.[3,4] The introduction of polyatomic cluster ion sources (e.g. Au_n^+, Bi_n^+, C_{60}^+) has expanded the capabilities of this technique, opening new possibilities for the analysis of biological materials[5–9] and, consequently, the application of ToF-SIMS in geobiology and organic geochemistry.[10–12] A most advantageous property of ToF-SIMS is its ability to record the intensities of any detected ion in a given area of interest at a microscopic scale.[13] To date, this is not possible with any of the extract-based techniques routinely used in biomarker studies, namely GC/MS and LC/MS (coupled gas chromatography/mass spectrometry, coupled liquid chromatography/mass spectrometry). Whereas GC/MS and LC/MS are effective tools for the identification and quantification of organic compounds, it remains difficult to link the chemical information obtained to specific structures of interest in heterogeneous and structurally complex biological or geological materials. In ToF-SIMS, identification of organic compounds is achieved mainly through precise mass determination, sometimes corroborated by the analysis of the lateral distribution of the species of interest in selected areas on the sample surface. However, the absence or as yet sparse number of published ToF-SIMS spectral fragmentation patterns may hamper an accurate structural assignment. Likewise, the influence of the chemical environment (matrix) on the ionisation of molecules and their fragmentation appears to be an important factor,[14] but is still not well explored.

Studies performed previously on reference compounds of widespread hydrocarbon biomarkers[15–17] showed that ToF-SIMS spectra may, or may not, differ considerably from those obtained with conventional mass spectrometric techniques (see also[3]). By comparison with pure reference compounds, it was recently proven possible to detect hydrocarbon biomarkers, namely hopanes and steranes, in crude oils by ToF-SIMS.[12] Recent studies on animal tissues, eukaryotic cells or microbial consortia also revealed the potential of ToF-SIMS with cluster ion sources for investigating the distribution of intact lipids in natural samples.[6,9,10,18,19] Whereas these studies focused on materials with a more or less pre-characterised

*Correspondence to: C. Heim, Geobiology Group, Geoscience Centre, University of Göttingen, Goldschmidtstraße 3, D-37077 Göttingen, Germany.
E-mail: cheim@gwdg.de
Contract/grant sponsor: German Research Foundation (DFG); contract/grant number: Th 713/4 and FOR 571.
Contract/grant sponsor: The University of Hamburg (joint project BEBOP, R/V Poseidon cruise PO 317/2.
Contract/grant sponsor: The Swedish Governmental Agency for Innovation Systems (VINNOVA).

lipid content, the authors pointed out that the establishment of ToF-SIMS reference data is a major prerequisite for the investigation of organic molecules in barely studied or unknown environmental materials.

This study presents previously unpublished ToF-SIMS spectra of eight functionalised glycerolipids as important members of cell membrane constituents of eukaryotes, bacteria, and archaea. These lipids, or their derivatives, are commonly used as biomarkers in geo- and microbiology, organic geochemistry, and microbial ecology.[6,9,10,18,19] Our work aims to provide basic information about the ToF-SIMS fragmentation patterns of these compounds in both, positive and negative ion modes. In addition to 'conventional' ester-bound glycerolipids, we also included a number of ether-bound counterparts, as such compounds may reveal important information on the protagonists in some microbially driven ecosystems.[20] Emphasis was placed not only on high (molecular) mass species, but also on characteristic fragments that may enable a robust identification of the respective molecule, or the compound class, in a natural sample. However, detectability of a pure reference substance does not necessarily imply that the compound can be easily identified by the same features when analysed in a complex chemical matrix. To assess the possibility of detecting such lipids in natural samples and the influence of matrix effects, ToF-SIMS spectra of selected glycerolipids (archaeol, phosphoglycerol, diglyceride) were therefore compared with those recorded from the same, or related, compounds in an organic extract and in cryosections of microbial mats.

EXPERIMENTAL

Eight commercially available glycerolipids (Avanti Lipids, Sigma, Chiron) were selected for analysis, namely; (i) L-*α*-phosphatidylethanolamine (GPEtn), (ii) 1,2 di-*O*-hexadecyl-*sn*-glycero-3-phosphatidylethanolamine (Diether-GPEtn), (iii) L-*α*-phosphatidylcholine (GPCho), (iv) 1,2-di-*O*-dialkyl-*sn*-glycerol-3-phosphatidylcholine (Diether-GPCho), (v) L-*α*-phosphatidylglycerol (GPGro), (vi) 1-palmitoyl-2-oleoyl-*sn*-glycerol (DG), (vii) 1,2-di-*O*-hexadecyl-*rac*-glycerol (Diether-DG), and (vii) 1,2-di-*O*-phytanyl-*sn*-glycerol (archaeol), see Table 1.

All reference lipids were stored cold and dark in glass vials with Teflon septa before, and between, analyses. Each reference lipid (1 mg) was dissolved in 1 mL pre-distilled solvents (dichloromethane, *n*-hexane). For ToF-SIMS analysis, the compounds were deposited on silicon wafers. The wafers were rinsed with deionised water and cleaned in a UV ozone apparatus prior to use in order to remove any organic contaminants from the surface. Using a glass pipette, a few μL of each lipid solution (except for GPCho, see below) were placed on a silicon wafer and the organic solvent was allowed to evaporate. The deposition processes were carried out in a laminar air flow cabinet in order to avoid airborne particulate contamination. The GPCho sample was prepared as a supported lipid bilayer, according to Prinz *et al*.[25] As controls, blank silicon wafers were exposed to the same conditions during sample preparation, and analysed in parallel. To assess the presence of contaminants, ToF-SIMS spectra were also obtained from the evaporation residues of

Table 1. Glycerolipids studied and ions observed in the molecular weight range

Compound	Abbreviation	Formula	Exact mass	Observed $[M+H]^+$	Observed $[M+Na]^+$	Observed $[M-H]^-$	Others	
L-*α*-Phosphatidylethanolamine	GPEtn (16:0/18:2)	$C_{39}H_{74}NO_8P$	715.52	716.53	738.53	714.52	697.51	$[M-NH_3]^-$
L-*α*-Phosphatidylethanolamine	GPEtn (18:2/18:2)	$C_{41}H_{74}NO_8P$	739.52	740.55	762.54	738.52	—	—
1,2 Di-*O*-Hexadecyl-*rac*-phosphatidylethanolamine	Diether-GPEtn	$C_{37}H_{78}NO_6P$	663.56	664.65	—	662.49	624.67	$[M+Na-C_2H_8NO]^-$
L-*α*-Phosphatidylcholine	GPCho	$C_{42}H_{82}NO_8P$	759.58	760.61	782.61	—	744.54	$[M-CH_3]^-$
							699.47	$[M-C_3H_9N]^-$
1,2-*O*-Dialkyl-*sn*-glycero-3-phosphatidylcholine	Diether-GPCho	$C_{40}H_{85}NO_6P$	705.60	706.75	—	704.57	690.54	$[M-CH_3]^-$
							645.47	$[M-C_3H_9N]^-$
L-*α*-Phosphatidylglycerol (sodium salt)	GPGro	$C_{38}H_{74}O_{10}PNa$	744.49	—	767.51	721.58	721.58	$[M-Na]^-$
1-Palmitoyl-2-oleoyl-*sn*-glycerol	DG	$C_{37}H_{70}O_5$	594.52	595.58	617.53	593.49	577.52	$[M-H_2O]^+$
1,2 Di-*O*-hexadecyl-*rac*-glycerol	Diether-DG	$C_{35}H_{72}O_3$	540.55	541.63	563.58	539.54	522.59	$[M-H_2O]^+$
1,2-Di-*O*-phytanyl-*sn*-glycerol	Archaeol	$C_{43}H_{88}O_3$	652.67	653.72	675.68	651.66	634.69	$[M-H_2O]^+$

DOI: 10.1002/rcm

the pure solvents. These spectra were used as internal controls for a clean sample processing and are not shown here. Typically, sets of six samples were mounted on a sample holder and introduced into the vacuum chamber of the ToF-SIMS instrument immediately after preparation.

A sample of an iron-oxidising microbial mat dominated by *Gallionella ferruginea*[21] was obtained from a subterranean fluid discharge at −150 m depth in the Äspö Tunnel, SE Sweden. The mats were stored at −20°C prior to analysis.

A sample of a methanotrophic microbial mat was retrieved from the GHOSTDABS methane seep field on the NW' Black Sea shelf from a water depth of 230 m (joint project BEBOP, see Acknowledgements). These microbial mats have been studied in detail for their lipid biomarker patterns.[10,22–24] An organic extract of the Black Sea microbial mat was prepared as it would be typically done for LC/MS and GC/MS analyses. An aliquot of each mat (10 mg) was extracted with 15 mL of dichloromethane/methanol (3:1, 1:1, 1:3) in a Teflon-capped glass vial (ultrasonication, 20 min). After evaporation of the solvent mixture and re-dissolution in pure dichloromethane, the extracts were deposited on silicon wafers and were transferred to the ToF-SIMS instrument as described above.

For the preparation of the cryosections, the Black Sea and the *Gallionella* microbial mats were allowed to thaw at room temperature, and a small amount (approx. 10 mm^3) of each mat sample was mounted on a cork sample holder using an embedding agent (Cryo-Gel®, Electron Microscopy Sciences, PA, USA). The samples were frozen for 30 s in cold methyl butane at −150°C and immediately transferred into the cryochamber of a Leica CM 3050 S cryomicrotome (Leica Microsystems, Wetzlar, Germany) that had been pre-cooled to −20°C. Using a standard steel knife (Leica Profile D), serial sections of ca. 8 μm thickness were cut, deposited on standard microscope slides (76 × 26 mm), and stored at −20°C in closed glass containers until analysis. Prior to transfer into the ToF-SIMS instrument, the slides were allowed to approach room temperature with the glass container kept closed, in order to avoid condensation of water vapor on the sample.

All glassware (microscope slides, pipettes, vials, beakers, glass containers) was heated to 400°C for 2 h prior to use, and/or cleaned by thoroughly rinsing with deionised water and acetone. Solvent rinsing was also used to clean all steelware (spatula, tweezers, microtome knives) prior to use.

ToF-SIMS images and spectra of positive and negative ions were recorded using a ToF-SIMS IV instrument (ION-TOF GmbH, Münster, Germany) equipped with a liquid bismuth cluster ion source. Data were acquired in bunched mode with a mass resolution of ca. M/ΔM 5000, using 25 keV Bi_3^+ primary ions at a pulsed current of 0.1 pA. Low-energy electron flooding was used for charge compensation, when necessary. The analysed areas were 100 × 100 μm^2 or 200 × 200 μm^2 for references and extracts, and 500 × 500 μm^2 for the microbial mat cryosections. The areas were scanned in a raster pattern at 128 × 128 pixels for reference lipids and extracts, and 256 × 256 pixels for the cryosections. The acquisition times were typically between 50 s and 100 s for the pure lipid reference samples and the extracts, and 300 s to 500 s for the cryosections. All analyses were thus done under so-called static SIMS condition, i.e. with primary ion doses well below those where significant surface damage due to the ion bombardment starts to appear.[11]

RESULTS AND DISCUSSION

Through comparison of the spectra from the different lipids, it was possible to determine characteristic peaks and fragmentation schemes for the respective lipid classes. In the low-mass range, fragments specifying phospholipids in general were *m/z* 78.95 $[PO_3]^-$ and 96.97 $[H_2PO_4]^-$, as previously reported (e.g.[6,19]). In addition, other distinctive headgroup fragments are present in the spectra of particular phospholipid classes. Such fragments where reproducibly detected in both ester- and ether-bound phospholipids and are listed in Table 2. Fragmentation of ester-bound lipids leads to prominent peaks of the corresponding fatty acid chains whereas the ether-bound lipids exhibited weak fragment ion peaks of the alcohol side chains (Table 2). In general, the fragmentation tendency of ether lipids is considerably lower compared to ester-bound lipids, probably due to the higher chemical stability of the ether link.

Phosphatidylethanolamine (GPEtn): $C_{39}H_{74}NO_8P$; exact mass 715.52 Da (Da); source: eukaryotes,[9,19] bacteria.[27]

Molecular ions are detected at *m/z* 716.53 and 740.55 in the positive spectrum. Whereas the former is in accordance with the $[M+H]^+$ ion of the actual GPEtn molecule containing one $C_{16:0}$ and one $C_{18:2}$ moiety ($C_{16:0}/C_{18:2}$), the latter seems to originate from GPEtn that carries two $C_{18:2}$ chains ($C_{18:2}/C_{18:2}$). The observed distribution is in good agreement with the product specification from the distributor ($C_{16:0} = 24\%$, $C_{18:2} = 60\%$). Both molecular ions produce sodium adducts $[M+Na]^+$ at *m/z* 738.53 and 762.54, respectively. Characteristic fragments in positive mode are observed at *m/z* 575.49 $[M–headgroup]^+$, 306.29 and 282.28 (Table 1) and are interpreted to result from cleavage within the glycerol backbone (see fragmentation scheme, Fig. 1 and Table 2). Specific headgroup fragments are observed at *m/z* 142.03 and 182.06 corresponding to $[C_2H_9NO_4P]^+$ and $[C_5H_{13}NO_4P]^+$.

In negative mode, deprotonated molecular ions $[M–H]^-$ occur at *m/z* 714.55 ($C_{16:0}/C_{18:2}$) and 738.55 ($C_{18:2}/C_{18:2}$). Ions at *m/z* 697.51 and 671.48 are interpreted as $[M–NH_3]^-$ and $[M–C_2H_7N]^-$. Prominent peaks at *m/z* 96.97 $[H_2PO_4]^-$ and 78.96 $[PO_3]^-$ (not shown) and at *m/z* 140.02 clearly specify the phosphate-bearing headgroup, as observed in previous studies.[18,19] Fragments at *m/z* 279.25 ($C_{18:2}$) and 255.24 ($C_{16:0}$) can be assigned to fatty acid chains (according to[18]), whereas fragments at *m/z* 476.29, 452.29 and 434.28 putatively derive from the PE molecule after loss of the fatty acid chains as indicated in Fig. 1.

1,2-Di-*O*-hexadecyl-*sn*-glycero-3-phosphatidylethanolamine (Diether-GPEtn): $C_{37}H_{78}NO_6P$; exact mass 663.56 Da; source: bacteria.[31]

The positive mass spectrum observed for Diether-GPEtn reveals a weak protonated molecular ion $[M+H]^+$ at *m/z* 664.65 (Fig. 2). A single, most prominent and possibly diagnostic peak occurs at *m/z* 624.67. It is tentatively interpreted as a fragment ion resulting from loss of the ethanolamine group and adduction of Na $[M–C_2H_7NO+Na]^+$ (Fig. 2). Another, less

DOI: 10.1002/rcm

Table 2. Characteristic fragments and headgroup ions

Abbreviation	Formula	Charactristic fragment ions (+) observed*	Tentative formula	Characteristic fragment ions (−) observed*	Tentative formula	Headgroup ions (+) observed*	Formula	Headgroup ions (−) observed*	Formula
GPEtn ($C_{16:0/18:2}$)	$C_{39}H_{74}NO_8P$	575.49	$C_{37}H_{67}O_4^+$	279.25	$C_{18}H_{31}O_2^-$	142.03	$C_2H_9NO_4P^+$	140.02	$C_2H_7NO_4P^-$
		282.28	$C_{18}H_{34}O_2^+$	255.24	$C_{16}H_{31}O_2^-$	182.06	$C_5H_{13}NO_4P^+$	180.04	$C_5H_{11}NO_4P^-$
GPEtn ($C_{18:2/18:2}$)	$C_{41}H_{74}NO_8P$	599.50	$C_{39}H_{67}O_4^+$	279.25	$C_{18}H_{31}O_2^-$	142.03	$C_2H_9NO_4P^+$	140.02	$C_2H_7NO_4P^-$
		306.29	$C_{20}H_{34}O_2^+$			182.06	$C_5H_{13}NO_4P^+$	180.04	$C_5H_{11}NO_4P^-$
Diether-GPEtn	$C_{37}H_{78}NO_6P$	??	??	239.21	$C_{16}H_{31}O^-$	—	—	180.04	$C_2H_7NO_4P^-$
								140.01	$C_5H_{11}NO_4P^-$
GPCho	$C_{42}H_{82}NO_8P$	504.38	$C_{26}H_{51}NO_6P^+$	281.24	$C_{18}H_{33}O_2^-$	184.10	$C_5H_{15}NO_4P^+$	—	—
		478.37	$C_{24}H_{49}NO_6P^+$	255.23	$C_{16}H_{31}O_2^-$	166.08	$C_5H_{13}NO_3P^+$		
Diether-GPCho	$C_{40}H_{85}NO_6P$	464.44	$C_{24}H_{51}NO_5P^+$	239.21	$C_{16}H_{31}O^-$	184.11	$C_5H_{15}NO_4P^+$	—	—
		450.41	$C_{23}H_{49}NO_5P^+$						
GPGro	$C_{38}H_{74}O_{10}PNa$	551.52	$C_{35}H_{67}O_4^+$	255.24	$C_{16}H_{31}O_2^-$	198.99	$C_3H_6Na_2O_5P^+$	171.04	$C_3H_8O_6P^-$
		511.28	$C_{22}H_{42}Na_2O_8P^+$					211.06	$C_6H_{12}O_6P^-$
								153.02	$C_3H_6O_5P$
DG	$C_{37}H_{70}O_5$	339.31	$C_{21}H_{39}O_3^+$	281.24	$C_{18}H_{33}O_2^-$	—	—	91.04	$C_3H_7O_3^-$
		313.28	$C_{19}H_{37}O_3^+$	255.23	$C_{16}H_{31}O_2^-$				
		265.26	$C_{18}H_{33}O^+$						
		239.24	$C_{16}H_{31}O^+$						
Diether-DG	$C_{35}H_{72}O_3$	297.32	$C_{19}H_{37}O_2^+$	241.23	$C_{16}H_{33}O^-$	—	—	91.02	$C_3H_7O_3^-$
		299.33	$C_{19}H_{39}O_2^+$	239.19	$C_{16}H_{31}O^-$				
		253.27	$C_{17}H_{33}O^+$						
Archaeol	$C_{43}H_{88}O_3$	373.39	$C_{23}H_{49}O_3^+$	371.37	$C_{23}H_{47}O_3^-$	—	—	91.03	$C_3H_7O_3^-$
		371.27	$C_{23}H_{47}O_3^+$	297.32	$C_{20}H_{41}O^-$				
				295.29	$C_{20}H_{41}O^-$				

* [19] described further, yet unknown negative ions at *m/z* 137, 153 and 181 as common phospholipid fragments. These findings were partly confirmed in our study. Both fragments at 137.01 and 153.02 were found in the ester-bound phospholipids, whereas the ether-bound phospholipids yielded *m/z* 137.01. An ion at *m/z* 181 was not observed in our spectra. Further positive ions described by [19], at *m/z* 125, 143 and 165, were exclusively observed in the spectrum of GPGro (Na salt) and may represent Na-containing fragments.

DOI: 10.1002/rcm

RCM

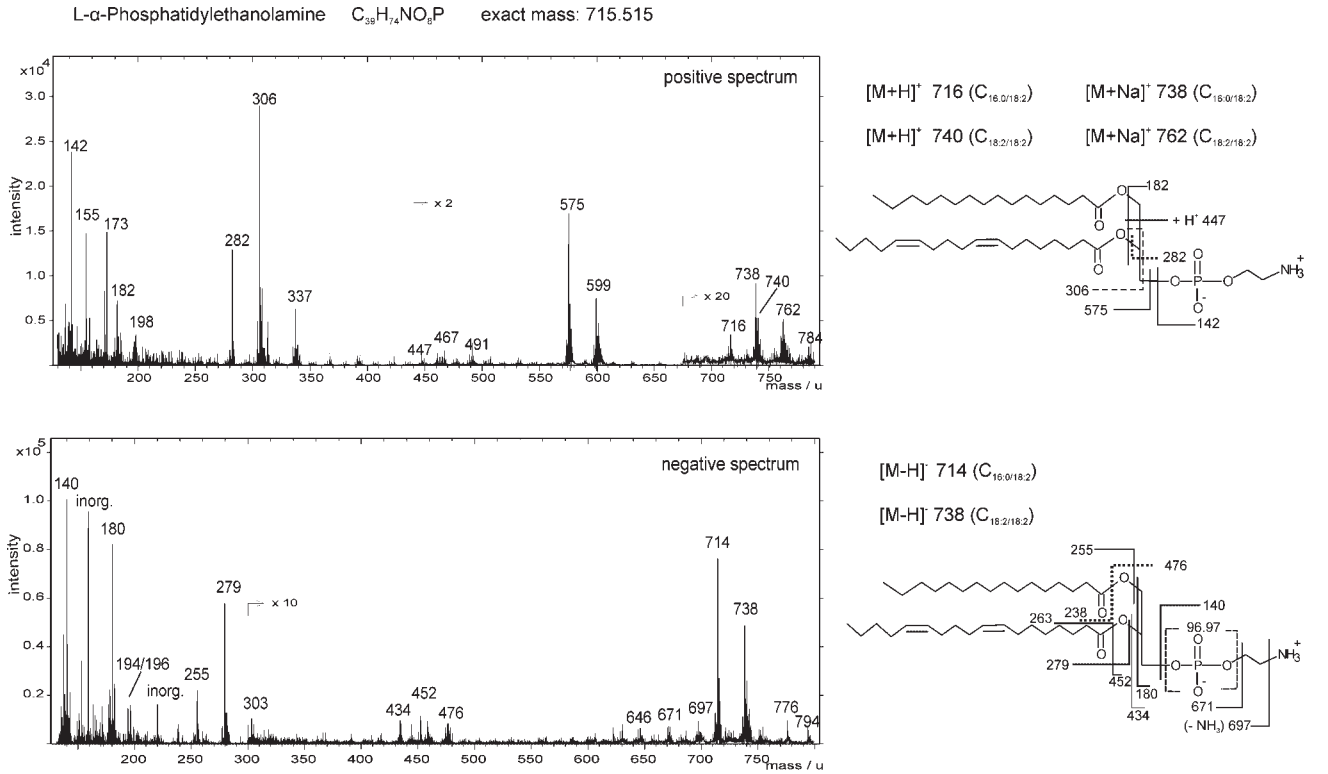

Figure 1. Partial positive (top) and negative (bottom) ToF-SIMS spectra (*m/z* 140–800) of phosphatidylethanolamine (GPEtn). This reference standard mainly contains GPEtn carrying two $C_{18:2}$ or each one $C_{16:0}$ and $C_{18:2}$ fatty acid chains ($C_{16:0} = 24\%$; $C_{18:2} = 60\%$ of the total fatty acids). See text for a detailed discussion of the spectral patterns. The prominent phosphate peak at *m/z* 96.97 is out of the displayed range. Peaks labeled with 'inorg' are inorganic ions and do not belong to the compound spectrum.

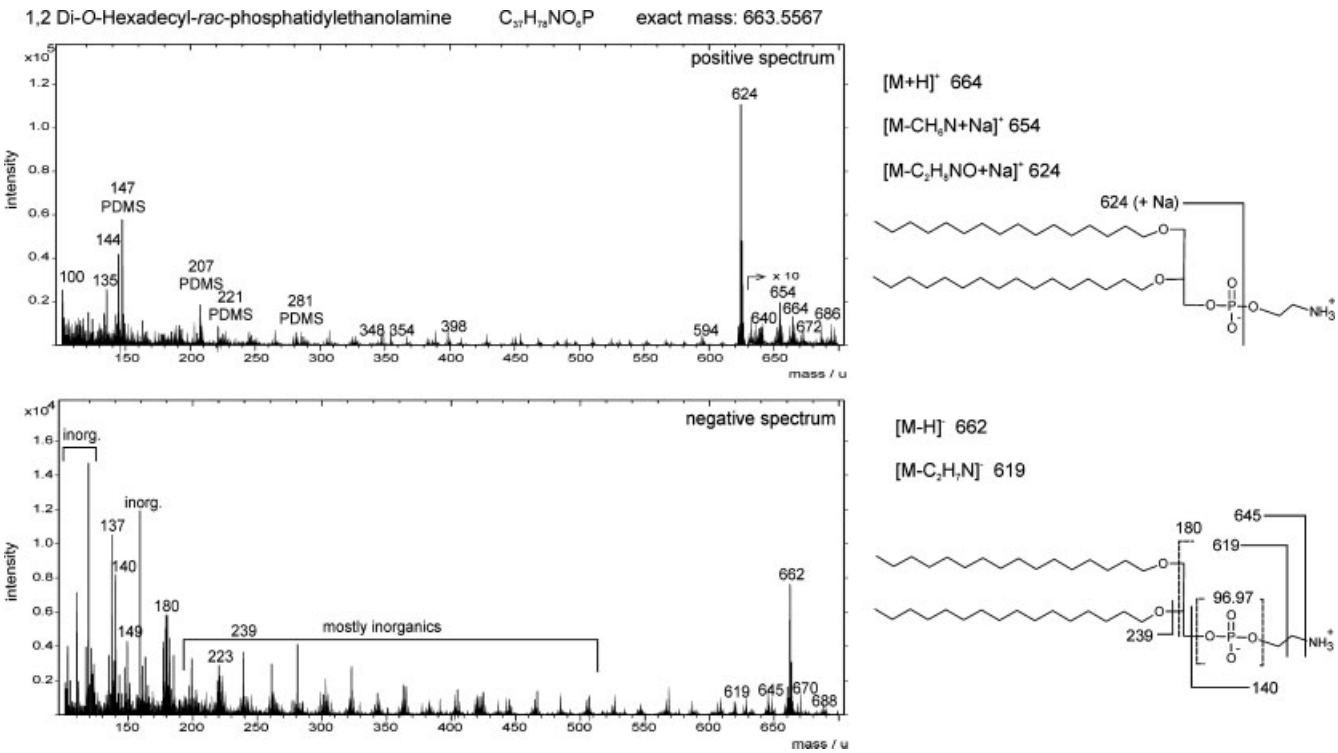

Figure 2. Partial positive (top) and negative (bottom) ToF-SIMS spectra (*m/z* 100–700) of 1,2-di-*O*-hexadecyl-*sn*-glycero-3-phosphatidylethanolamine (Diether-GPEtn). See text for a detailed discussion of the spectral patterns. Peaks labeled with inorganics are contaminant ions and do not belong to the compound spectrum.

DOI: 10.1002/rcm

RCM

abundant sodium adduct of a fragment ion may occur at *m/z* 654.68 $[M–CH_6N+Na]^+$.

The negative spectrum shows a clear deprotonated molecular ion $[M–H]^-$ at *m/z* 662.49. In addition, minor fragments at *m/z* 645.47 and 619.46 can be interpreted as $[M–NH_3]^-$ and $[M–C_2H_7N]^-$, respectively. It is interesting to see that in both positive and negative mode, peaks expected from lyso-fragments or aliphatic side chains (around *m/z* 224) are weak or even missing. Likewise, headgroup fragments of Diether-GPEtn are only observed in the negative spectrum (Fig. 2, Table 1). Generally, the fragmentation pattern of Diether-GPEtn is less prominent than that observed for ester-bound GPEtn (Fig. 1). This is interpreted as reflecting the greater stability of the ether compared to the ester linkage, which appears to hamper rearrangement reactions and cleavage of the side chains under primary ion bombardment.

L-α-Phosphatidylcholine (GPCho): $C_{42}H_{82}NO_8P$; exact mass 759.58 Da; source: eukaryotes,[6,9,19] bacteria.[32]

Weak molecular ions of GPCho are detected as $[M+H]^+$ and $[M+Na]^+$ at *m/z* 760.61 and 782.61 in the positive spectrum (Fig. 3). Similarly, abundant peaks of Lyso-GPCho fragments occur at *m/z* 478.37 and 504.38. The most prominent peaks in the positive GPCho spectrum are observed at *m/z* 166.08 and 184.10 and correspond to the headgroup fragments $[C_5H_{13}NO_3P]^+$ and $[C_5H_{15}NO_4P]^+$.

The negative spectrum of GPCho does not show a deprotonated molecular ion. Instead, characteristic fragments at *m/z* 744.54 and 699.47 can be assigned to $[M–CH_3]^-$ and $[M–C_3H_9N]^-$. Ions at *m/z* 255.23 and 281.24 derive from $C_{16:0}$ and $C_{18:1}$ fatty acid moieties, respectively.

The relatively low intensities of the molecular ions and characteristic higher mass fragments make it difficult to use these ions for the analysis of intact GPCho in environmental samples. Furthermore, it has been reported that the intensity of the molecular ion peak is highly sensitive to the structural configuration of the lipid, showing higher intensity in bilayer structures as compared to disordered structures,[25] making the lack of a molecular ion a somewhat uncertain indicator for the absence of GPCho. Although the detection of molecular GPCho ions has been reported in tissue samples,[6] the headgroup fragment (*m/z* 184.07) provides a strong and characteristic peak for phosphocholine-containing lipids and is therefore frequently used for mapping of these lipids in cell and tissue samples.[18,26] Comparison of the ToF-SIMS spectra of GPEtn and GPCho with published ToF-SIMS and electrospray ionisation (ESI) (LC/MS) mass spectra of phosphatidylcholine[18,19,27] suggests similar principles for the fragmentation of complex ester-bound phospholipids. Beside the molecular ion, both methods yield fragment peaks, phospholipid headgroup ions in positive and negative spectra as well as the fatty acid chains in the negative spectra, which may be used to corroborate structural identification.

1,2-O-Dialkyl-*sn*-glycerol-3-phosphatidylcholine (Diether-GPCho): $C_{40}H_{85}NO_6P$; exact mass 705.60 Da; source: bacteria.[31]

Unlike ester-bound GPCho, Diether-GPCho produces a prominent $[M+H]^+$ ion at *m/z* 706.75 (Fig. 4). Weak fragment ions occur in the positive spectrum at *m/z* 450.41, 464.44, 480.42 and 494.47, and may originate from the cleavage of one alkyl moiety at different positions close to the respective ether bond (Fig. 4). A rather prominent doublet of fragment ions at *m/z* 224.15/226.13 can be plausibly explained by loss of both side chains.

In the positive spectrum of Diether-GPCho, the phosphocholine (PC) headgroup fragment is clearly identified at *m/z* 184.11 (Fig. 4). The observed formation of a strong PC

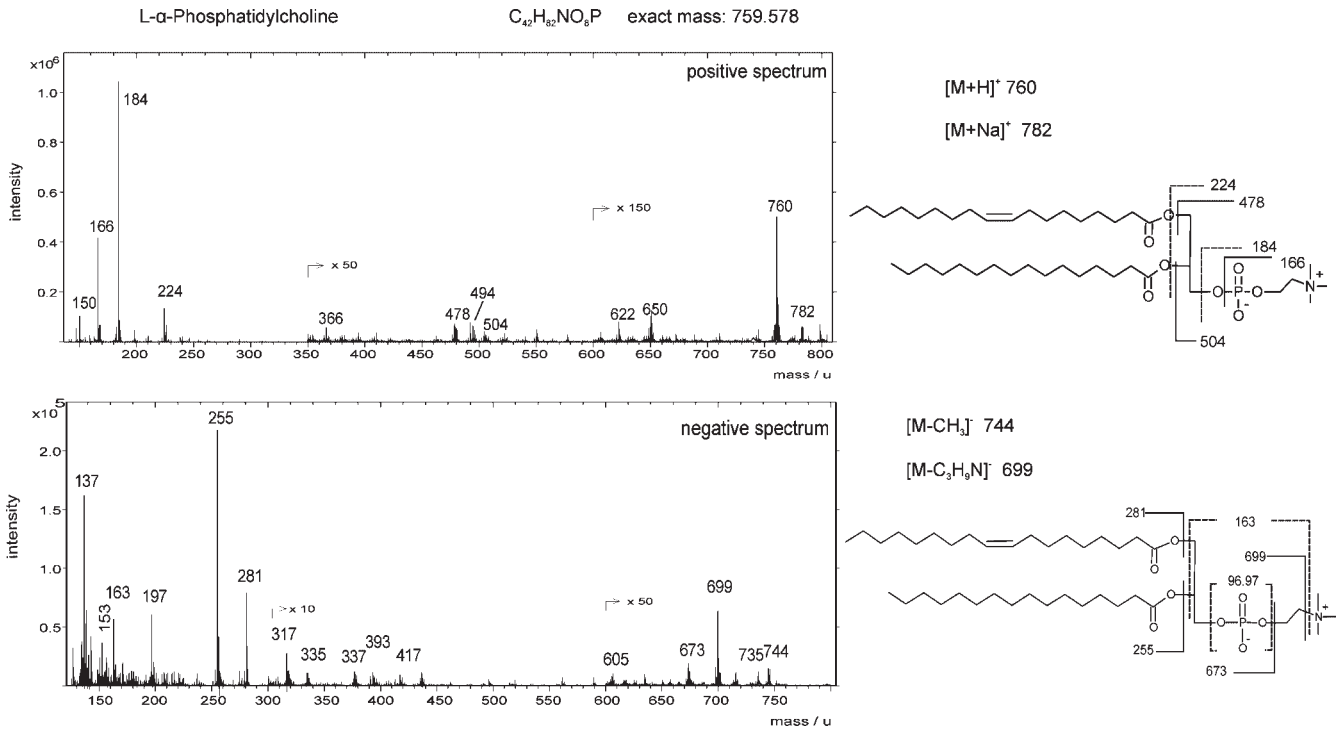

Figure 3. Partial positive (top) and negative (bottom) ToF-SIMS spectra (*m/z* 130–800) of L-α-phosphatidylcholine (GPCho). See text for a detailed discussion of the spectral patterns.

DOI: 10.1002/rcm

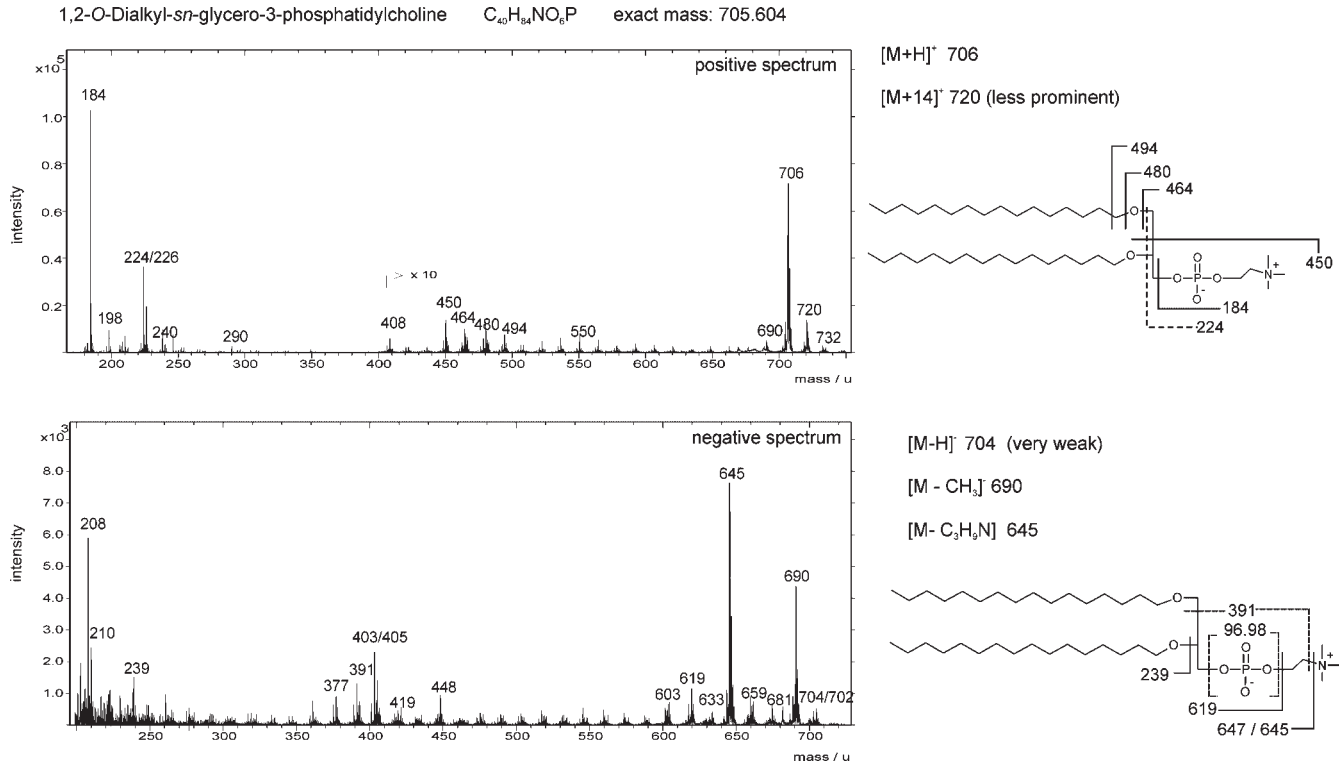

Figure 4. Partial positive (top) and negative (bottom) ToF-SIMS spectra (*m/z* 170–750) of 1,2-*O*-dialkyl-*sn*-glycerol-3-phosphocholine (Diether-GPCho). See text for a detailed discussion of the spectral patterns.

fragment is in good agreement with the results obtained from the ester-bound GPCho (Fig. 3) and other lipid studies that used the PC headgroup fragment at *m/z* 184.11 for GPCho identification in ToF-SIMS spectra of animal cells and tissues.[6,18]

The negative spectrum of Diether-GPCho shows a very weak $[M–H]^-$ peak at *m/z* 704.57, whereas strong fragment ions occur at *m/z* 690.54, 645.47 and 619.47. These fragments most probably result from the molecule after loss of a methyl group from the trimethylamine moiety of the PC, $[M–CH_4]^-$, loss of the trimethylamine moiety, $[M–C_3H_9N]^-$, or loss of the entire PC headgroup, respectively. Notably, this pattern differs considerably from the counterpart lipid with an ethanolamine headgroup (Diether-GPEtn, see above) that shows $[M–H]^-$ as the most prominent peak in the molecular mass range. Fragment ions at *m/z* 391.24, 403.24/405.25 and 448.29 may result from cleavage of the hexadecyl chain, with or without loss of C-1 of the glycerol, and the trimethylamine moiety of the PC headgroup.

L-α-Phosphatidylglycerol (GPGro) sodium salt: $C_{38}H_{74}O_{10}PNa$; exact mass 744.49 Da; source: eukaryotes,[19] bacteria.[27,32] GPGro sodium salt produces a prominent $[M+Na]^+$ ion at *m/z* 767.51 in the positive spectrum (Fig. 5). A protonated molecule $[M+H]^+$ was not observed. Due to the high abundance of sodium, the GPGro fragments including the headgroup are charged with an additional Na^+ ion, e.g. *m/z* 511.28 ($C_{22}H_{42}Na_2O_8P^+$) and 198.99 ($C_3H_6Na_2O_5P^+$). Prominent peaks at 124.94, 142.96 and 164.94 are putatively Na^+ adducts.

Beside the weak deprotonated GPGro molecule $[M–H]^-$ at *m/z* 721.58, the ion at *m/z* 255.24 represents the $C_{16:0}$ fatty acid moiety. Peaks at *m/z* 153.02, 171.04 and 211.06 can be assigned as fragments involving the PG headgroup. The occurrence of a strong fragment at *m/z* 153.02 is in good agreement with observations reported for ESI-MS.[27] However, for this fragment, Mazalla *et al*.[27] proposed a precursor ion at *m/z* 227, which was not observed in the ToF-SIMS spectra. Ions at *m/z* 211.06, 171.04 and 153.02 suggest a preferred fragmentation within the glycerol backbone of the GPGro rather than a scission of the glycerol headgroup (Fig. 5), as observed for other ester-bound phospholipids (GPEtn, Fig. 1, and GPCho, Fig. 3).

1-Palmitoyl-2-oleoyl-*sn*-glycerol (DG): $C_{37}H_{70}O_5$; exact mass 594.52 Da; source: eukaryotes,[28,29] bacteria.[32]

DG produces very weak molecular ion peaks $[M+H]^+$ and $[M+Na]^+$ at *m/z* 595.58 and 617.53, but a prominent $[M–H_2O]^+$ ion at *m/z* 577.52 (Fig. 6). Distinct positive ions at *m/z* 339.31, and 313.28 represent lyso fragments of DG, whereas *m/z* 265.26 and 239.24 may originate from fatty acyl fragments.

In the negative spectrum of DG, a weak molecular ion $[M–H]^-$ is detected at *m/z* 593.49. Strong fatty acid fragments are observed at *m/z* 281.24 ($C_{18:1}$) and 255.23 ($C_{16:0}$).

It should be considered that triacylglycerides (TG) were reported to produce a prominent DG fragment ($[M–H_2O]^+$) in the positive spectrum.[28,29] Moreover, this fragment was clearly visible in the GPEtn spectrum (Fig. 1, Table 2) and was detectable, though in low abundance, in the spectra of other ester-bound lipids studied. Hence, when analysing natural samples, positive and negative spectra and ion images have to be checked carefully, whether the respective ions can be assigned confidently to DG, TG or phospholipids.

DOI: 10.1002/rcm

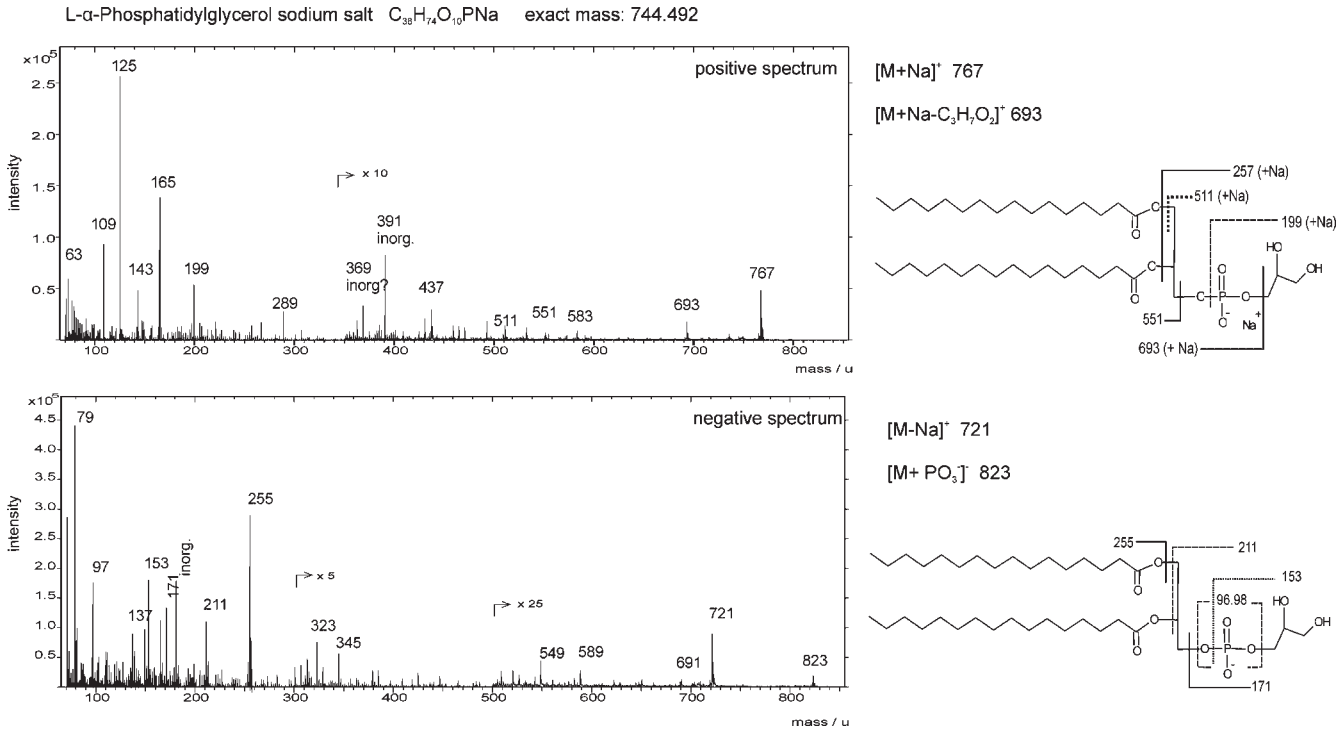

Figure 5. Partial positive (top) and negative (bottom) ToF-SIMS spectra (*m/z* 50–850) of L-α-phosphatidylglycerol sodium salt (GPGro). Peaks labeled 'inorg' are inorganic ions and do not belong to the compound spectrum. See text for a detailed discussion of the spectral patterns.

1,2-Di-*O*-hexadecyl-*rac*-glycerol (Diether-DG): $C_{37}H_{72}O_3$; exact mass 540.55 Da; source: bacteria.[20]

The partial positive spectrum of 1,2-di-*O*-hexadecyl-*rac*-glycerol (Diether-DG) shows the protonated molecular ion at *m/z* 541.63 as the base peak (Fig. 7). Loss of the functional group with, or without, the C-3 of glycerol produces additional, less intense peaks at *m/z* 522.59 and 508.57, respectively. Further ions at *m/z* 253.27, 267.29, 297.32 and 299.33 can be explained by fragmentations within the glycerol backbone whereas *m/z* 317.34 most likely results from loss of one of the hydrocarbon side chains $[M–C_{16}H_{31}]^+$ (Table 2).

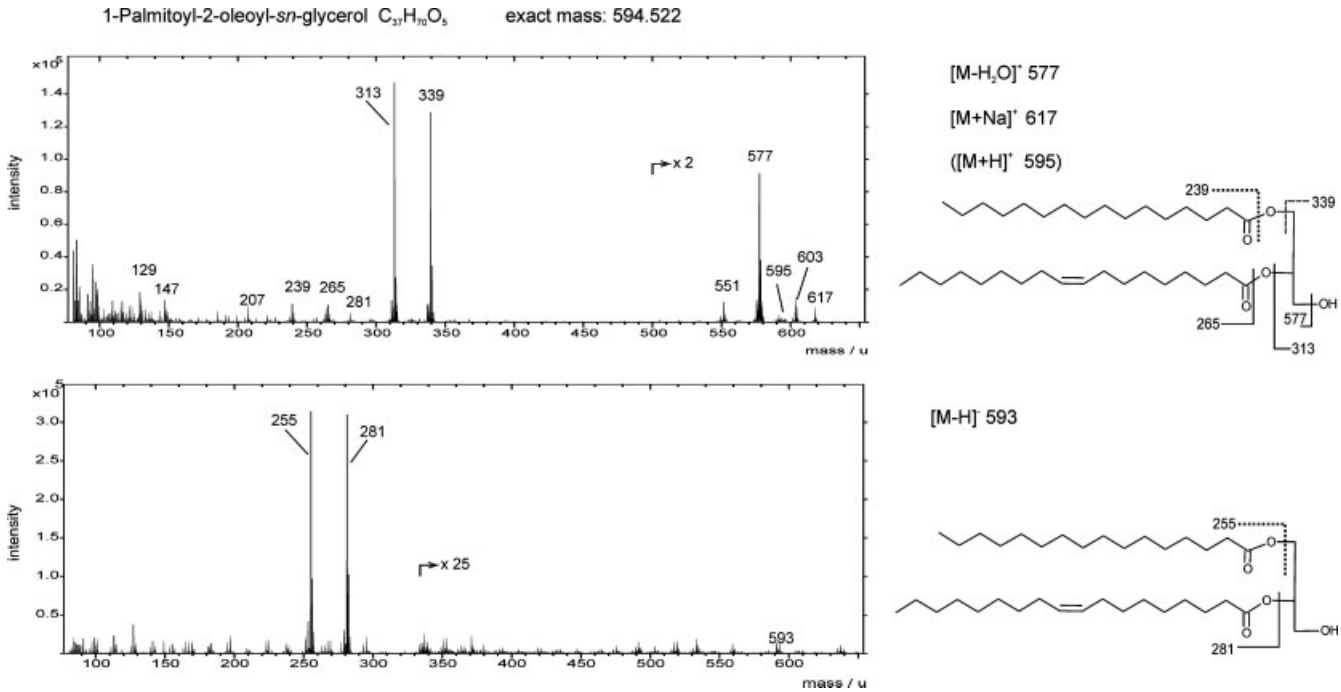

Figure 6. Partial positive (top) and negative (bottom) ToF-SIMS spectra (*m/z* 80–650) of 1-palmitoyl-2-oleoyl-*sn*-glycerol (DG). See text for a detailed discussion of the spectral patterns.

DOI: 10.1002/rcm

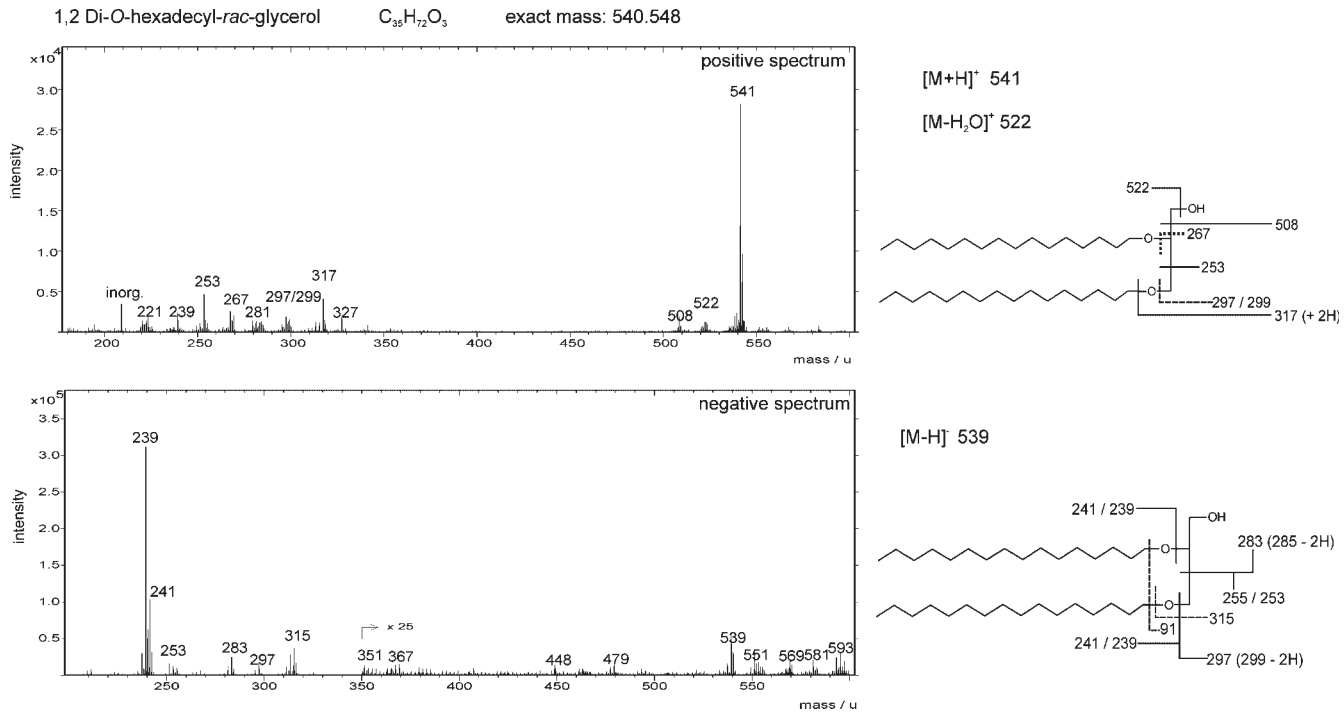

Figure 7. Partial positive (top) and negative (bottom) ToF-SIMS spectra (*m/z* 180–600) of 1,2-di-*O*-hexadecyl-*rac*-glycerol (Diether-DG). See text for a detailed discussion of the spectral patterns. Peaks labeled 'inorg' are inorganic ions and do not belong to the compound spectrum.

In the negative spectrum, the deprotonated molecular ion at *m/z* 539.54 $[M–H]^-$ is very weak, as also observed for the isoprenoid glycerol diether archaeol (see below). The most abundant ion in the higher molecular weight range at *m/z* 239.18 most probably derives from the side chain $[C_{16}H_{31}O]^-$. This interpretation is supported by a corresponding, 56 Da heavier, fragment ion observed in the negative spectrum of archaeol at *m/z* 295.29 (see below), that obviously represents the functionalised C_{20} phytanyl side chain $[C_{20}H_{39}O]^-$. Similar to the positive spectrum, minor ions at *m/z* 253.20, 255.20, 283.22 and 297.28 indicate fragmentations within the glycerol backbone of Diether-DG. Another significant ion at *m/z* 315.26 most likely results from loss of one of the hydrocarbon side chains $[M–C_{16}H_{33}]^-$, again corroborated by a 56 Da heavier corresponding fragment observed in the negative spectrum of archaeol (*m/z* 371.25). The presence of a glycerol moiety in the Diether-DG molecule is recognised by a prominent $C_3H_7O_3$ fragment ion peak at *m/z* 91.03 (not shown).

1,2-Di-*O*-phytanyl-*sn*-glycerol (archaeol): $C_{43}H_{88}O_3$; exact mass 652.67 Da; source: archaea.[23,30]

The positive spectrum of archaeol displays the protonated molecular ion $[M+H]^+$ at *m/z* 653.72 as the base peak (Fig. 8). The formation of a Na^+ adduct causes a further, yet minor, peak at *m/z* 675.68. Loss of the hydroxyl group (as H_2O) from the glycerol moiety is the most plausible explanation for a fragment peak at *m/z* 634.69 whereas cleavage of the adjacent methyl group results in a peak at *m/z* 620.65. The fragmentation scheme of archaeol producing ions at *m/z* 620.65, 373.39, 371.27 and 278.23 is similar to the peak formation in GC/MS (data not shown).

In the negative ToF-SIMS spectrum, a deprotonated molecular ion $[M–H]^-$ at *m/z* 651.66 is clearly recognised, though much weaker than the $[M+H]^+$ ion observed in positive mode. Pronounced fragment ions occur at *m/z* 371.37, 297.32, 295.29, 239.07, 223.02 and 165.04. Whereas *m/z* 371.37, 297.32 and 295.29 can be explained by cleavage of the ether bonds, the latter three are due to polydimethylsiloxane (PDMS) contamination. Additional characteristic fragments contributing to clear identification of archaeol as a glycerolipid are the glycerol fragments at *m/z* 91.02 $[C_3H_7O_3]^-$ and 57.04 $[C_3H_5O]^-$ in the negative spectrum (data not shown).

Archaeol in a methanotrophic microbial mat

Extracts of the Black Sea microbial mats typically contain archaeol among other lipids derived from methanotrophic archaea.[22–24] Based on these findings, our group recently used ToF-SIMS to study the distribution of archaeal lipids, including intact glycerol tetraethers, in microscopic cryosections of the microbial mats.[10] Figure 9(a) shows partial positive ToF-SIMS spectra of (i) the archaeol reference (as described above), (ii) a total organic extract of a microbial mat, and (iii) a cryosection of the same mat. In fact, the molecular ion as $[M+Na]^+$ of archaeol (Fig. 9(a)) and some of its characteristic fragments such as *m/z* 371.27 and 373.37 were observed in the spectra of all samples (Fig. 9(b)). Unlike the reference lipid, the spectra of the extract and the cryosection show $[M+Na]^+$ at *m/z* 675.68, rather than $[M+H]^+$. Clearly, archaeol easily forms the $[M+Na]^+$ ion wherever sodium is present, either from biological material, sea water, or the mineral matrix of a natural sample. The same is evidently the case for the hydroxylated diether, hydroxyarchaeol (*m/z* 691.68), that co-occurs with archaeol in the Black Sea mats (Fig. 9(a); see also e.g.[22]). The strong tendency of these isoprenyl diethers to form sodium adduct ions is in full agreement with previous data,[30] thus pointing

DOI: 10.1002/rcm

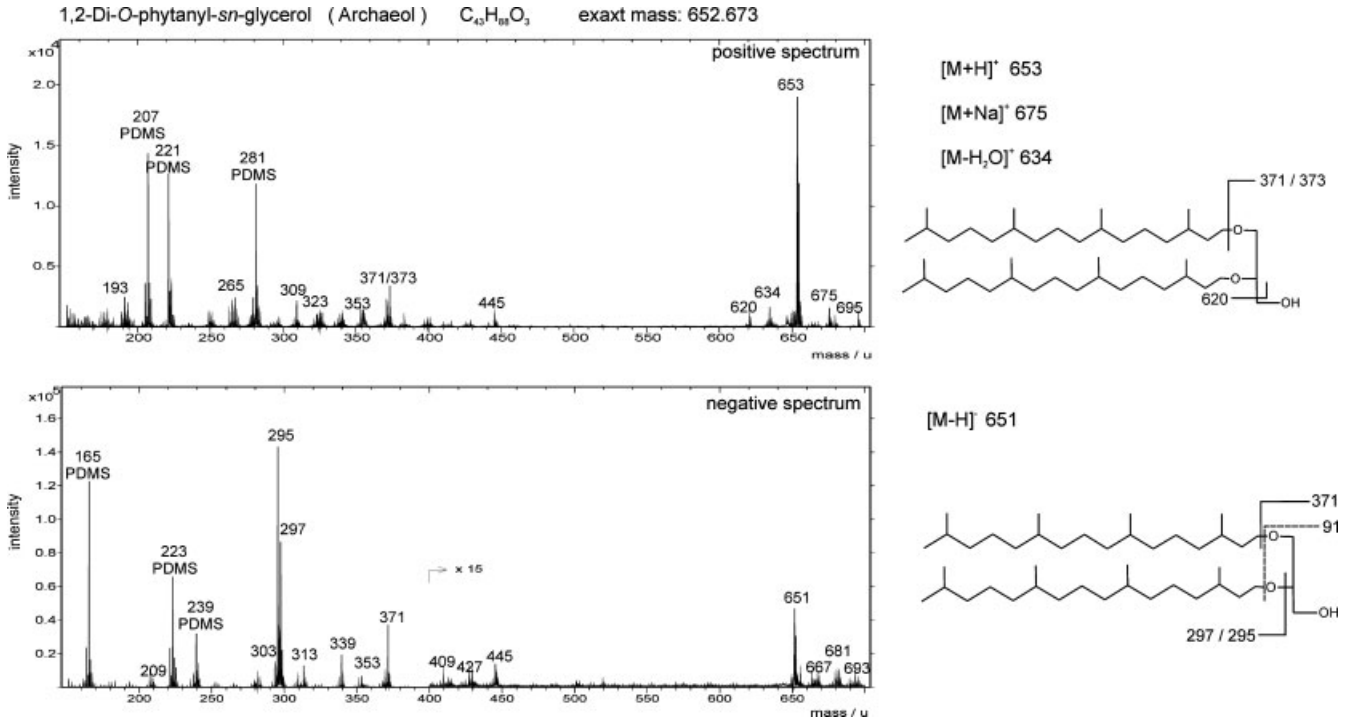

Figure 8. Partial positive (top) and negative (bottom) ToF-SIMS spectra (*m/z* 140–700) of 1,2-di-*O*-phytanyl-*sn*-glycerol (archaeol). See text for a detailed discussion of the spectral patterns. A peak at *m/z* 91.02 specifying the glycerol moiety is out of the displayed range of the negative spectrum. Peaks labeled with PDMS are polysiloxane contaminants and do not belong to the compound spectrum.

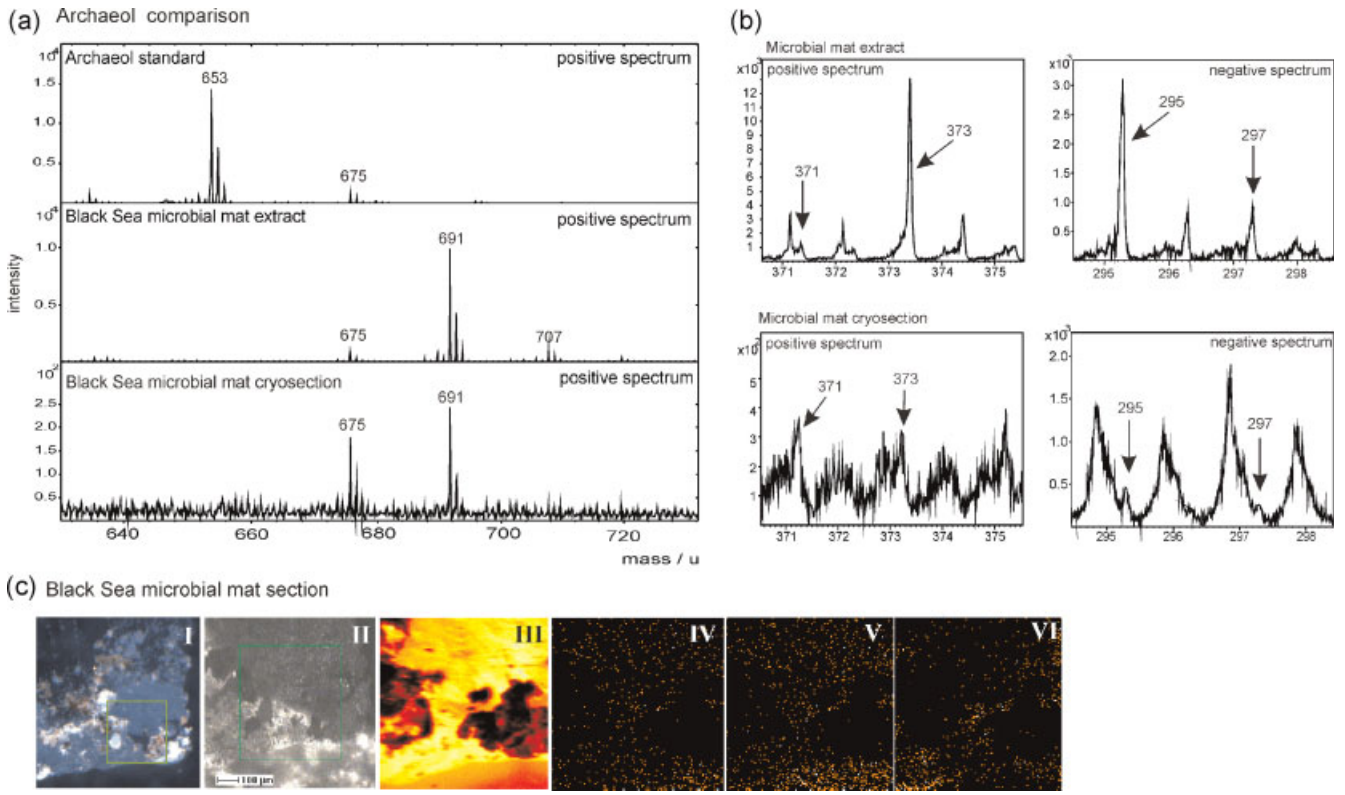

Figure 9. (a) Partial positive ToF-SIMS spectra (*m/z* 630–730) showing molecular ions ($[M+H]^+$ and $[M+Na]^+$) of archaeol from the standard, in a complex organic extract of the Black Sea microbial mat, and on a microscopic cryosection of the same microbial mat. The peaks at 691.67 and 707.65 Da in the environmental samples represent the $[M+Na]^+$ of hydroxyarchaeol and dihydroxyarchaeol, respectively. (b) Characteristic archaeol fragments observed in the partial positive and negative spectra of the organic extract and the microbial mat cryosection. (c) Microscopic and ion images of the Black Sea microbial mat section: under reflected light (I), built-in video camera in the ToF-SIMS system (II), total ion image (III), distribution of *m/z* 371.27 and 373.39 (IV), distribution of archaeol (V), and distribution of hydroxyarchaeol (VI).

DOI: 10.1002/rcm

at the reproducibility of the mass spectral patterns characterising these important lipid biomarkers.

Although the $[M+H]^+$ and $[M-H]^-$ ions were not detected in the spectra of the organic extract and the microscopic section of the Black Sea microbial mat, characteristic archaeol fragments at *m/z* 371.27 and 373.39 in the positive spectra and at *m/z* 295.29 and 297.32 in the negative spectra (described in Fig. 8) were clearly present (Fig. 9(b)). Thus, the co-occurrence of the $[M+Na]^+$ ion in positive mode and these fragment peaks in negative mode corroborate the identification of archaeol in the environmental sample. Microscopic, video and total ion images of the microscopic section (Fig. 9(c): I, II, III) allow the accurate assignment of the area analysed. IV, V and VI in Fig. 9(c) show positive ion images

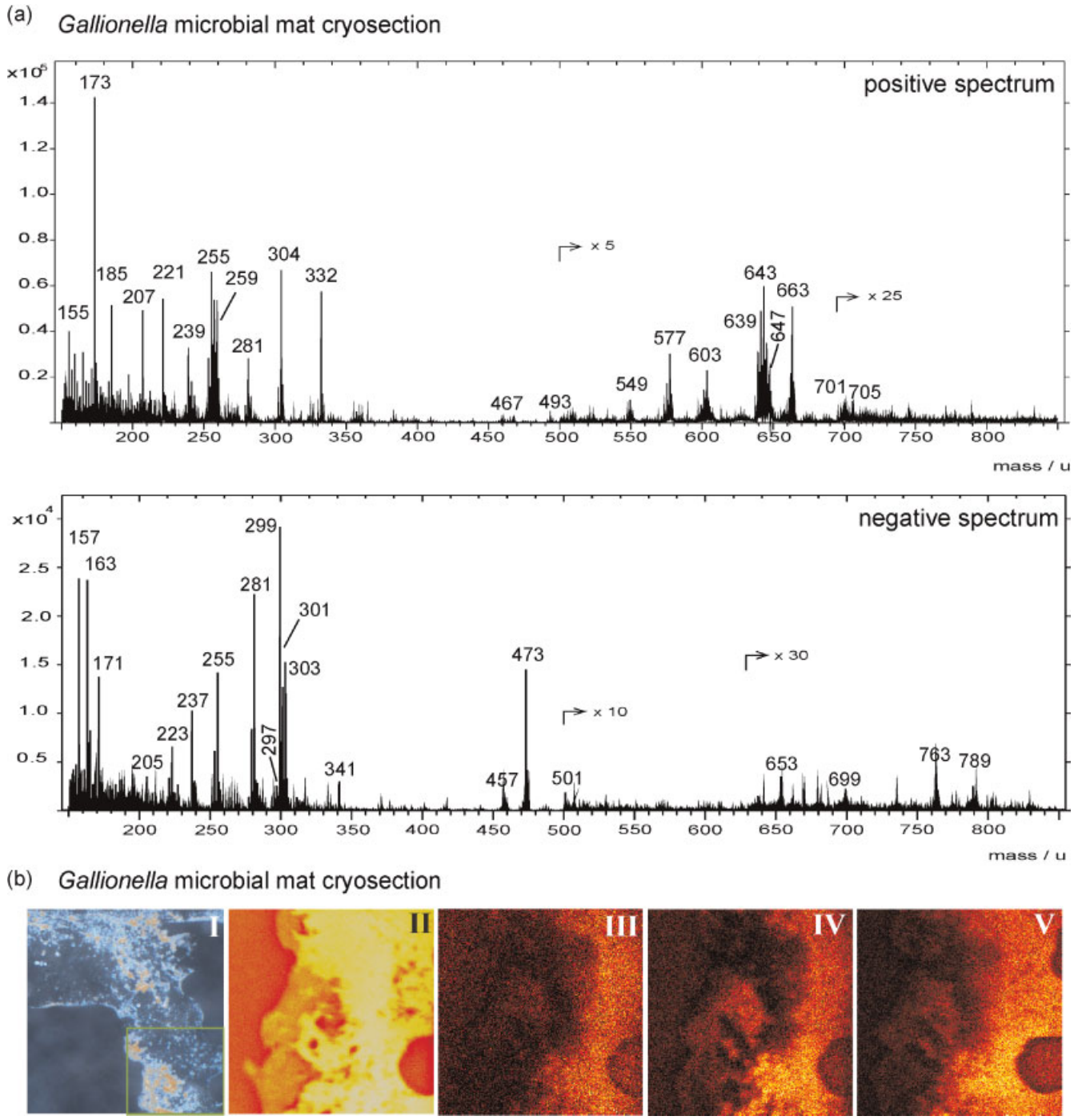

Figure 10. (a) Partial positive and negative ToF-SIMS spectra (*m/z* 150–850) of a microscopic section obtained from a *Gallionella*-rich microbial mat from the tunnel of Äspö. Peaks at *m/z* 207.04, 221.12 and 281.08 in the positive spectrum belong to PDMS contaminants, and peaks at *m/z* 647.47 and 663.47 in the positive spectrum and at *m/z* 473.28 in the negative spectrum most likely derive from contamination by the polymer additive Irgafos 168. The peaks at *m/z* 341.09 and 163.05 originate from carbohydrate fragments of the embedding agent. See text for a detailed discussion of the spectral patterns. (b) Microscopic and ion images of the *Gallionella* microbial mat section: under reflected light (I), total ion image (II), the distribution of the PG headgroup (III), fatty acids (IV), and diglycerides (V).

DOI: 10.1002/rcm

obtained from the microscopic section, proving the co-localisation of the fragment ions at *m/z* 371.27, 373.39 with the $[M+Na]^+$ ion of archaeol.

Diglycerides and phosphatidylglycerol in a *Gallionella*-dominated microbial mat

Generally, analyses of environmental samples of iron-oxidising *Gallionella* mats is hampered by obscuring effects caused by the iron oxide precipitates that commonly make up more than 90 wt% of the dry sample. It was nonetheless possible to reconstruct partially the lipid pattern of the microbial system using spectra and the imaging capability of ToF-SIMS (Fig. 10).

In the positive spectrum ions at *m/z* 549.50, 577.54, 603.55, 639.47 and 643.49 are in agreement with the $[M–H_2O]^+$ ions of diglyceride lipids namely $C_{32:1}$, $C_{34:1}$, $C_{36:2}$, $C_{40:12}$ and $C_{40:10}$. This assignment was corroborated through the fragmentation scheme of the DG reference (Fig. 6) including occurrence of a glycerol-derived fragment at *m/z* 91.02 $[C_3H_7O]^-$ and the corresponding fatty acyl moieties in the negative spectrum. Here, fragment ions at *m/z* 253.19 and 255.21 correspond to $C_{16:1}$ and $C_{16:0}$ moieties, whereas *m/z* 279.20 and 281.215 arise from $C_{18:2}$ and $C_{18:1}$ moieties, respectively. Additional ions at *m/z* 299.18, 301.19 and 303.21 are in agreement with hexaenoic, pentaenoic and tetraenoic C_{20} fatty acids, respectively. These fatty acids were also observed in GC/MS analyses of *Gallionella*-dominated mat bulk extracts (data not shown).

In the phospholipid molecular ion range in the negative spectrum, significant peaks at *m/z* 761.55, 763.56 and 789.57 were detected. A distinct ion at *m/z* 171.08 (negative spectrum) corresponding to the GPGro headgroup is also present. The high-mass peaks may therefore be related to the phosphatidylglycerols (GPGro), namely $C_{35:1}$, $C_{35:0}$ and $C_{37:1}$, thus implying the presence of odd-numbered fatty acyl moieties (Fig. 10(b)). Although the GPGro headgroup was co-localised with C_{17} and C_{19} fatty acids, this relationship remains uncertain, as the latter were observed only in minor abundance on the cryosections. Additional prominent organic ions such as *m/z* 332.33, 304.29 and 173.08 in the positive spectrum and *m/z* 237.06 and 157.11 in the negative spectrum still remain to be identified.

CONCLUSIONS

Our study showed that ToF-SIMS with a Bi cluster ion source is capable of revealing characteristic mass spectral features of each of the eight glycerolipids investigated. However, a robust assignment of the target compounds in the total ToF-SIMS spectrum of environmental samples should not only rely on the presence of molecular ions (including adducts), but also on specific headgroup fragments and other structural moieties, such as functional groups and alkyl chains. The establishment of characteristic mass spectral features for a range of glycerolipids further expands the range of complex lipids that can be analysed using ToF-SIMS and provides the crucial basis for the identification of these and related biomarkers in environmental materials. Nevertheless, the question whether the patterns reported here represent general rules for the interpretation of ToF-SIMS spectra of environmental samples still has to be corroborated by further studies.

A major advantage of ToF-SIMS is its capacity to provide simultaneous detection, identification and microscopic localisation (mapping) of inorganic and organic compounds without the need for bulk sample extraction or labeling. Unlike the more traditional techniques for lipid analysis such as GC/MS and LC/MS, ToF-SIMS can be used to study compound distributions within microscopic areas of interest on a sample surface. The imaging capacity of ToF-SIMS can also be used to support the identification of organic compounds and their association with inorganic species through the co-localisation of key ions on the area of interest. As the analytical procedure is virtually non-destructive, subsequent examinations, e.g. microscopy, may allow a further characterisation of the sample in question.

The capability of visualising lipid distributions on a micrometer scale makes ToF-SIMS a promising tool for a wide range of geological, ecological, biological, and medical applications. However, published ToF-SIMS spectra of lipid biomarkers as yet exist for a still limited number of relevant compounds, and little research has been conducted on the effects of substrates and compound concentrations on the quality of ToF-SIMS spectra. Furthermore, structural assignments using the current single-stage TOF analysers are still not satisfactory, and isomers cannot be easily differentiated. Moreover, SIMS is very susceptible to surface contamination.

Further efforts are therefore essential to minimise, or overcome, these limitations and further increase the utility of ToF-SIMS for molecular imaging in bio- and geosciences. Such efforts may include the implementation of tandem mass spectrometry, the improvement of preparation techniques particularly for environmental samples, the establishment of further reference data from pure substances, and the validation of the ToF-SIMS results against established knowledge and methods.

Acknowledgements

We are grateful to Michael Wiedenbeck and Jan Toporski for their constructive reviews that greatly helped to improve the original manuscript. The authors acknowledge Jakob Malm (SP Borås) for constructive discussions and help in the lab. We are also grateful to Walter Michaelis, Richard Seifert (University of Hamburg) and Joachim Reitner (University of Göttingen), who initiated and coordinated the joint projects through which the microbial mats studied here were retrieved. Our study received financial support from the German Research Foundation (DFG) through grants Th 713/4 and FOR 571, the University of Hamburg (joint project BEBOP, R/V Poseidon cruise PO 317/2), and the Swedish Governmental Agency for Innovation Systems (VINNOVA). This is publication no. 46 of the DFG Research Unit FOR 571 'Geobiology of Organo- and Biofilms'.

REFERENCES

1. Benninghoven A. *Angew. Chem. Int. Edn Engl.* 1994; **33**: 1023.
2. Pacholski ML, Winograd N. *Chem. Rev.* 1999; 2977.
3. Vickerman JC, Briggs D (eds). *ToF-SIMS: Surface Analysis by Mass Spectrometry*, IM Publications and Surface Spectra Limited, 2001.
4. Belu AM, Graham DJ, Castner G. *Biomaterials* 2003; **24**: 3635.

DOI: 10.1002/rcm

5. Kollmer F. *Appl. Surf. Sci.* 2004; **231**: 153.
6. Sjövall P, Lausmaa J, Johansson B. *Anal. Chem.* 2004; **76**: 4271.
7. Touboul D, Halgand F, Brunelle A, Kersting R, Tallarek E, Hagenhoff B, Laprévote O. *Anal. Chem.* 2004; **76**: 1550.
8. Touboul D, Kollmer F, Niehuis E, Brunelle A, Laprevote O. *J. Am. Soc. Mass Spectrom.* 2005; **16**: 1608.
9. Ostrowski SG, Van Bell CT, Winograd N, Ewing AE. *Science* 2004; **305**: 71.
10. Thiel V, Heim C, Arp G, Hahmann U, Sjövall P, Lausmaa J. *Geobiology* 2007; **5**: 413.
11. Sjövall P, Thiel V, Siljeström S, Heim C, Hode T, Lausmaa J. *Geostandards Geoanal. Res.* 2008; **32**: 267.
12. Siljeström S, Hode T, Lausmaa J, Sjövall P, Toporski J, Thiel V. *Org. Geochem.* 2009; **40**: 135.
13. Hagenhoff B. *Mikrochim. Acta* 2000; **132**: 259.
14. Sostarecz AG, Cannon DM, McQuaw CM Jr, Sun S, Ewing AG, Winograd N. *Langmuir* 2004; **20**: 4926.
15. Steele A, Toporski JKW, Avci R, Guidry S, McKay DS. *Org. Geochem.* 2001; **32**: 905.
16. Toporski JKW, Steele A. *Org. Geochem.* 2004; **35**: 793.
17. Toporski JKW, Steele A, Westall F, Avci R, Martill DM, McKay DS. *Geochim. Cosmochim. Acta* 2002; **66**: 1773.
18. Börner K, Malmberg P, Månsson J-E, Nygren H. *Int. J. Mass Spectrom.* 2007; **260**: 128.
19. Ostrowski SG, Szakal C, Kozole J, Roddy TP, Xu J, Ewing AE, Winograd N. *Anal. Chem.* 2005; **77**: 6190.
20. Pancost RD, Bouloubassi I, Aloisi G, Sinninghe Damsté JS. *Org. Geochem.* 2001; **32**: 695.
21. Pedersen K. *FEMS Microbiol. Rev.* 1997; **20**: 399.
22. Blumenberg M, Seifert R, Reitner J, Pape T, Michaelis W. *Proc. Natl. Acad. Sci.* 2004; **101**: 11111–11116.
23. Pape T, Blumenberg M, Seifert R, Egorov VN, Gulin SB, Michaelis W. *Palaeogeography, Palaeoclimatology, Palaeoecology* 2005; **227**: 31.
24. Michaelis W, Seifert R, Nauhaus K, Treude T, Thiel V, Blumenberg M, Knittel K, Gieseke A, Peterknecht K, Pape T, Boetius A, Amann R, Jorgensen BB, Widdel F, Peckmann JR, Pimenov NV, Gulin MB. *Science* 2002; **297**: 1013.
25. Prinz C, Hook F, Malm J, Sjövall P. *Langmuir* 2007; **23**: 8035.
26. Nygren H, Börner K, Hagenhoff B, Malmberg P, Månsson J-E. *Biochim. Biophys. Acta* 2005; **1737**: 102.
27. Mazalla N, Molinet J, Syakti AD, Dodi A, Bertrand J-C, Doumenq P. *Rapid Commun. Mass Spectrom.* 2005; **19**: 3579.
28. Malmberg P, Nygren H, Richter K, Chen Y, Dangardt F, Friberg P, Magnusson Y. *Microsc. Res. Techniq.* 2007; **70**: 828.
29. Nygren H, Malmberg P. *Trends Biotechnol.* 2007; **25**: 499.
30. Thiel V, Toporski J, Schumann G, Sjövall P, Lausmaa J. *Geobiology* 2007; **5**: 75.
31. Rütters H, Sass H, Cypionka H, Rullkötter J. *Arch. Microbiol.* 2001; **176**: 435.
32. Zink K-G, Wilkes H, Disko U, Elvert M, Horsfield B. *Org. Geochem.* 2003; **34**: 755.

DOI: 10.1002/rcm